ARMY RESEARCH LABORATORY

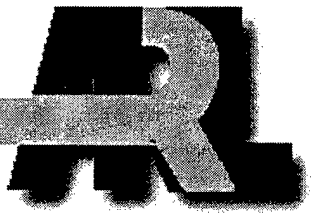

Current and Heat Transport in a Double Taper Sabot-Armature

John D. Powell
Alexander E. Zielinski

ARL-TR-2523 JULY 2001

The findings in this report are not to be construed as an official Department of the Army position unless so designated by other authorized documents.

Citation of manufacturer's or trade names does not constitute an official endorsement or approval of the use thereof.

Destroy this report when it is no longer needed. Do not return it to the originator.

Army Research Laboratory
Aberdeen Proving Ground, MD 21005-5066

ARL-TR-2523 July 2001

Current and Heat Transport in a Double Taper Sabot-Armature

John D. Powell
Alexander E. Zielinski
Weapons & Materials Research Directorate

Abstract

A model developed previously to investigate the transport of electromagnetic fields and energy in solid-armature railguns is simplified to exclusively study heating within the interior of the armature. A particular type of armature is then specifically studied, and the effect of variation of a number of parameters that affect its geometry is investigated. Results of the calculations are studied carefully and explained by basic physical principles. Some indication of how the results and conclusions can be used to influence design criteria for armatures is also indicated.

ACKNOWLEDGMENTS

The authors are indebted to Dr. James F. Newill of the U.S. Army Research Laboratory for his careful review of the final manuscript.

INTENTIONALLY LEFT BLANK

Contents

Figures

Tables

INTENTIONALLY LEFT BLANK

CURRENT AND HEAT TRANSPORT IN A
DOUBLE TAPER SABOT-ARMATURE

1. Introduction

In previous work (Powell, Walbert, & Zielinski 1993), we developed a two-dimensional (2-D) model for investigating the coupled effects of electromagnetic field transport and heat transport in solid-armature railguns. The model has been extended on several occasions in recent years, and studies have been undertaken for various types of armatures (Powell & Zielinski 1995a, 1995b, 1997, 1999). These studies have enhanced our understanding of how force and thermal loading depend on geometry, how velocity affects the manner in which current is conducted, and how basic physical phenomena can be used to influence design criteria. More recently, results from the model calculations have been employed in structural dynamics codes to predict the response of both the armature and the rails to the effects of electromagnetic acceleration (Newill, Zielinski, & Powell 2001).

A schematic diagram of a cross section of a railgun, which has a simple rectangular armature, is shown in Figure 1. The two dimensions shown are the actual dimensions treated in the calculation. Current, conducted in the direction indicated by the arrows, produces a magnetic induction field $\vec{B}$ (which points out of the page) in the inner bore of the gun. This induction field interacts with the current in the armature via the standard Lorentz force to accelerate the projectile down the barrel of the gun. Current initially flows along the inside surfaces of both the rails and the armature, but it eventually diffuses into the interior of those conductors. The intent of the model calculations is to determine the temporal and spatial distribution of the electromagnetic fields, current density, and energy within the armature and rails.

Models similar to the one discussed here have been developed in the past and summarized extensively in earlier work. The most closely related work was probably the 2-D analysis undertaken by Long with both analytical (1986) and finite element (1987) models. Those models did much to expand our understanding of how various parameters affected the operation of the railgun. Later, finite element models were developed in three dimensions by Rodger, Leonard, and Eastman (1991) and by Hsieh (1995). The model by Hsieh, known as EMAP3D, has been undergoing particularly active development during the last decade approximately and offers promise for explaining many outstanding problems in railgun dynamics.

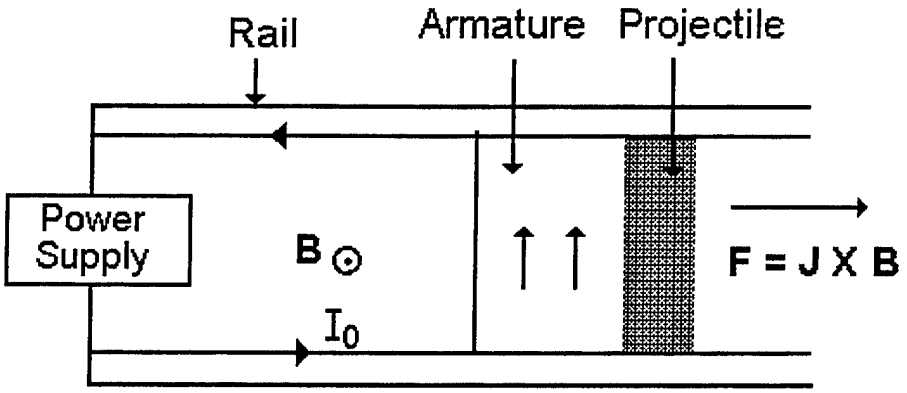

Figure 1. Schematic Diagram of Railgun.

In the present work, we develop a simplification of our previous models, which will be used exclusively to examine current and heat transport in the armature. The rails are not considered in the calculations. Consequently, we do not account for important phenomena, such as the velocity skin effect, that occur at the rail-armature interface. While accounting for these effects is clearly necessary in modeling the complete launch problem, neglecting them is probably satisfactory, provided we confine our attention to a region that is well within the interior part of the armature. The rationale for adopting this simplification is that it provides a mechanism by which calculations can be done in a reasonably simple way and in a reasonably short time.

We will furthermore confine our attention to a type of armature known to be of great value in launching high density tactical payloads. An illustration of the cross section of such an armature, derived from engineering criteria, is shown in Figure 2a (Zielinski 2001); a more detailed but schematic illustration of what is actually modeled is shown in Figure 2b. The armature has reflection symmetry about the centerline at $y = 0$ so that it is necessary to consider only the upper half. The left-hand face is formed by two lines, L_1 and L_2, which make angles α and β with the horizontal, and by an arc of radius r_0. The center of the arc is at the point (x_0,y_0), and lines L_1 and L_2 are tangent to the arc at the points (x_1,y_1) and (x_2,y_2). The upper left-hand corner of the armature is taken, for convenience, to be at $x = 0$, whereas the lower left-hand corner is at $x = x_3$. Current is conducted across the centerline at $y = 0$, throughout the interior of the armature, and across the top at $y = h$. We are interested in determining how a variation in certain dimensional parameters affects the spatial and temporal distribution of electromagnetic fields, electromagnetic forces, and energy within the interior of the armature.

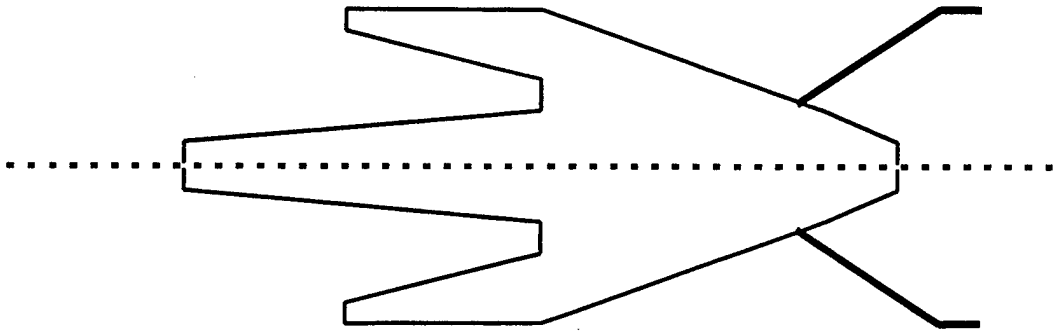

a. Illustration of cross section.

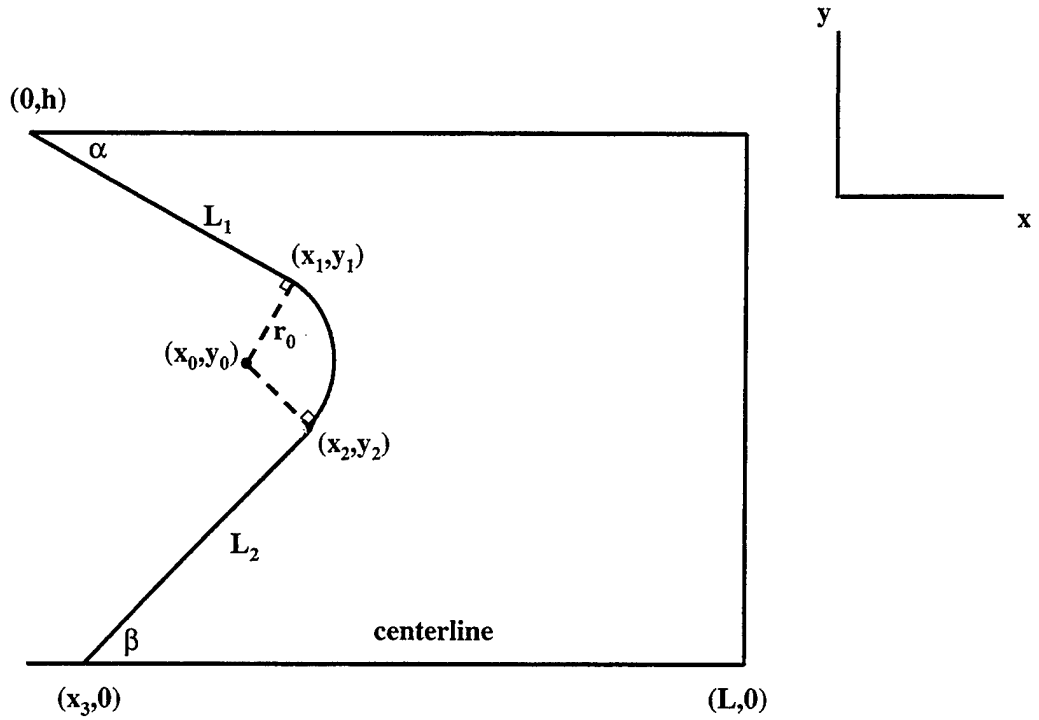

b. Schematic depicting details of the model.

Figure 2. Armature Employed in the Analysis.

The organization of the report is as follows. In Section 1, we describe the model in some detail and derive the governing equations that need to be solved. In Section 3, we present and compare results of some specific calculations in which the input parameters α, β, and r_0 are varied in a range of values. In Section 4, we present conclusions and indicate specific problems that require further study.

2. Model and Governing Equations

As indicated previously, we employ a simplification of the model that we have used before to study current and heat transport in the armature and rails for solid-armature railguns. The model is two dimensional in the *x-y* plane, as shown in Figure 1. We are interested in determining the electromagnetic fields as well as the temperature within the armature as a function of both space and time. The armature carries a total current per unit height (i.e., distance along the rail in the *z* direction) given by *j(t)*. That current enters at the bottom at $y = 0$ and leaves at the top at $y = h$.

2.1 Governing Equations and Boundary Conditions

As in previous work, it is convenient to work in a frame of reference in which the armature is at rest. The basic equations that determine the electromagnetic fields and temperature consist of Maxwell's equations as well as an energy conservation equation. Let $\vec{B}, \vec{E}$, and $\vec{J}$ be the magnetic induction, the electric field intensity, and the current density, respectively. Let μ and σ be the magnetic permeability and the electrical conductivity, respectively. Then, from Maxwell's equations, we have

$$\nabla \times \vec{E} = -\frac{\partial \vec{B}}{\partial t}, \tag{1}$$

$$\nabla \times \vec{B} = \mu \vec{J}, \tag{2}$$

and

$$\vec{J} = \sigma \vec{E}. \tag{3}$$

Equations (1) and (2) are the standard Maxwell curl equations, and Equation (3) is Ohm's law. In writing Equation (2), we have neglected the displacement current. In general, this approximation is valid for the relatively large time scales in which these types of conduction problems occur.

In accordance with the symmetry conditions as well as the 2-D nature of the model, we assume that $J_z = 0$, $E_z = 0$, $\vec{B} = B\hat{a}_z$ and that none of the variables depend on the z coordinate. With these assumptions, it is possible to uncouple Equations (1) through (3) to produce a single, second order, differential equation that governs the diffusion of the induction field *B*. The result is

$$\mu\sigma \frac{\partial B}{\partial t} = \frac{\partial^2 B}{\partial x^2} + \frac{\partial^2 B}{\partial y^2} - \frac{1}{\sigma}\frac{\partial \sigma}{\partial T}\frac{\partial T}{\partial x}\frac{\partial B}{\partial x} - \frac{1}{\sigma}\frac{\partial \sigma}{\partial T}\frac{\partial T}{\partial y}\frac{\partial B}{\partial y}. \tag{4}$$

In obtaining the result, we have assumed that σ depends on position only through the temperature T.

To account for energy transport and ohmic heating, we assume for the energy conservation equation that

$$\rho C\frac{\partial T}{\partial t}=\kappa\frac{\partial^2 T}{\partial x^2}+\kappa\frac{\partial^2 T}{\partial y^2}+\frac{\partial \kappa}{\partial T}\left(\frac{\partial T}{\partial x}\right)^2+\frac{\partial \kappa}{\partial T}\left(\frac{\partial T}{\partial y}\right)^2+\frac{1}{\mu^2\sigma}\left[\left(\frac{\partial B}{\partial x}\right)^2+\left(\frac{\partial B}{\partial y}\right)^2\right]-E_L. \quad (5)$$

In this equation, ρ, C, and κ represent the density, specific heat, and thermal conductivity, respectively, and these variables are also assumed to be functions only of the temperature. The terms involving the induction field in the equation can be recognized as just J^2/σ and therefore correspond to the energy dissipated per unit volume and time as a result of ohmic heating. The term E_L represents the energy absorbed during melting and depends on the heat of fusion of the armature material. A specific form for this term is discussed subsequently. In writing the equation in this form, we have assumed that ohmic heating is the only source of energy generation and that thermal conduction is the only energy transport mechanism. As implied, melting is accounted for, but no other phase change is assumed to occur. It is evident that Equations (4) and (5) are coupled since the electrical conductivity depends on temperature, and the source term in the energy equation depends on the induction field.

Equations (4) and (5) are identical to those employed in our previous work, except that there are no terms that account for the relative motion of the armature and rails. The absence of any velocity effects is because the rails are not included in the calculation and because the equations are solved in the moving reference frame. The equations must be solved subject to boundary conditions on all sides of the armature. We assume that there is no transfer of heat from the armature to its surroundings so that at every surface we must have

$$\hat{n}\bullet\nabla T=0, \quad (6)$$

where $\hat{n}$ represents the unit normal to the surface in question. On the left-hand face of the armature, we assume that

$$B=\mu j, \quad (7)$$

and on the right-hand face that

$$B=0. \quad (8)$$

Along both the lower and upper surfaces, we assume that

$$\frac{\partial B}{\partial y} = 0. \tag{9}$$

With the exception of the conditions along the upper surface, these boundary conditions are similar to those that we have justified previously and employed in all our calculations. The conditions on the upper face, where in reality the armature is in contact with the rail, are not realistic. However, since we are primarily interested in analyzing heating at points well within the interior of the armature, we assume that the precise conditions at that interface do not greatly affect the results. For simplicity, we have chosen the conditions to be the same as those along the centerline at $y = 0$.

2.2 Coordinate Transformation

As in previous work, we find it convenient to transform the equations of the previous section to a coordinate system in which the space occupied by the armature is rectangular. Various transformations with various degrees of complexity are possible, but for this problem, we choose a simple algebraic transformation to new coordinates ξ and η given by

$$\begin{aligned} \xi &= \frac{L}{L-s}(x-s) \\ \eta &= y \\ \tau &= t \end{aligned} \tag{10}$$

where $s = s(y)$ represents the horizontal distance from $x = 0$ to the left-hand edge of the armature at some point y. It is evident that this transformation will map the left-hand edge of the armature into $\xi = 0$, while the right-hand edge is maintained at $\xi = L$. For the particular type of armature being considered, s is given explicitly by the relations

$$\begin{aligned} s &= \frac{(x_2 - x_3)}{y_2} y + x_3 \quad \text{for } y < y_2 \\ s &= x_0 + [r_0^2 - (y - y_0)^2]^{1/2} \quad \text{for } y_2 \le y \le y_1 \\ s &= \frac{h - y}{h - y_1} x_1 \quad \text{for } y > y_1. \end{aligned} \tag{11}$$

The coordinates x_1, x_0, y_2, and so forth denote coordinates of the points indicated in Figure 2b. In general, we only specify the parameters α, β, h, r_0, y_0, and L as input. The remaining parameters follow, however, from a geometrical analysis of Figure 2b; formulas for these quantities are given in Table 1.

Table 1. Coordinates of Points Indicated in Figure 1

Parameter	Formula in Terms of Input Parameters
x_0	$(h - y_0 - r_0 \cos\alpha)/\tan\alpha - r_0 \sin\alpha$
x_1	$(h - y_0 - r_0 \cos\alpha)/\tan\alpha$
y_1	$y_0 + r_0 \cos\alpha$
x_2	$(h - y_0 - r_0 \cos\alpha)/\tan\alpha - r_0 \sin\alpha + r_0 \sin\beta$
y_2	$y_0 - r_0 \cos\beta$
x_3	$(h - y_0 - r_0 \cos\alpha)/\tan\alpha - r_0 \sin\alpha + r_0 \sin\beta - (y_0 - r_0 \cos\beta)/\tan\beta$

Equations (4) and (5) are transformed to the new coordinates by the application of the chain rule to express derivatives with respect to x, y, and t in terms of derivatives with respect to ξ, η, and τ. After considerable algebra, we find that the equations become

$$\mu\sigma\frac{\partial B}{\partial\tau} = A^2\frac{\partial^2 B}{\partial\xi^2} + \psi^2\left(\frac{\partial s}{\partial y}\right)^2\frac{\partial^2 B}{\partial\xi^2} + \frac{\partial^2 B}{\partial\eta^2} - 2\psi\frac{\partial s}{\partial y}\frac{\partial^2 B}{\partial\xi\partial\eta} - \psi\frac{\partial^2 s}{\partial y^2}\frac{\partial B}{\partial\xi} -$$
$$\frac{2\psi}{L-s}\left(\frac{\partial s}{\partial y}\right)^2\frac{\partial B}{\partial\xi} - \frac{A^2}{\sigma}\frac{\partial\sigma}{\partial T}\frac{\partial T}{\partial\xi}\frac{\partial B}{\partial\xi} - \frac{\psi^2}{\sigma}\frac{\partial\sigma}{\partial T}\left(\frac{\partial s}{\partial y}\right)^2\frac{\partial T}{\partial\xi}\frac{\partial B}{\partial\xi} - \frac{1}{\sigma}\frac{\partial\sigma}{\partial T}\frac{\partial T}{\partial\eta}\frac{\partial B}{\partial\eta} + \tag{12}$$
$$\frac{\psi}{\sigma}\frac{\partial\sigma}{\partial T}\frac{\partial s}{\partial y}\frac{\partial T}{\partial\xi}\frac{\partial B}{\partial\eta} + \frac{\psi}{\sigma}\frac{\partial\sigma}{\partial T}\frac{\partial s}{\partial y}\frac{\partial T}{\partial\eta}\frac{\partial B}{\partial\xi}$$

and

$$\rho C\frac{\partial T}{\partial\tau} = \kappa A^2\frac{\partial^2 T}{\partial\xi^2} + \kappa\frac{\partial^2 T}{\partial\eta^2} - 2\psi\kappa\frac{\partial s}{\partial y}\frac{\partial^2 T}{\partial\xi\partial\eta} + \kappa\psi^2\left(\frac{\partial s}{\partial y}\right)^2\frac{\partial^2 T}{\partial\xi^2} - \kappa\psi\frac{\partial^2 s}{\partial y^2}\frac{\partial T}{\partial\xi} -$$
$$2\frac{\kappa\psi}{L-s}\left(\frac{\partial s}{\partial y}\right)^2\frac{\partial T}{\partial\xi} + A^2\frac{\partial\kappa}{\partial T}\left(\frac{\partial T}{\partial\xi}\right)^2 + \psi^2\frac{\partial\kappa}{\partial T}\left(\frac{\partial s}{\partial y}\right)^2\left(\frac{\partial T}{\partial\xi}\right)^2 + \frac{\partial\kappa}{\partial T}\left(\frac{\partial T}{\partial\eta}\right)^2 - \tag{13}$$
$$2\psi\frac{\partial\kappa}{\partial T}\frac{\partial s}{\partial y}\frac{\partial T}{\partial\eta}\frac{\partial T}{\partial\xi} + \frac{A^2}{\mu^2\sigma}\left(\frac{\partial B}{\partial\xi}\right)^2 + \frac{\psi^2}{\mu^2\sigma}\left(\frac{\partial s}{\partial y}\right)^2\left(\frac{\partial B}{\partial\xi}\right)^2 + \frac{1}{\mu^2\sigma}\left(\frac{\partial B}{\partial\eta}\right)^2 -$$
$$\frac{2\psi}{\mu^2\sigma}\frac{\partial s}{\partial y}\frac{\partial B}{\partial\eta}\frac{\partial B}{\partial\xi} - E_L.$$

In these equations, A and ψ are given by the relations

and

$$\psi = \frac{L - \xi}{L - s}. \tag{15}$$

Similar transformations must be applied to the boundary conditions, but those derivations are straightforward to perform.

2.3 Material Properties and Latent Heat

In all the calculations undertaken, the armature was assumed to be composed of aluminum (7075). Material properties were obtained from curve fits discussed previously (Powell & Zielinski 1997). In those fits, it was assumed that the specific heat C, the resistivity η_r, the thermal conductivity κ, and the density ρ could be represented as linear functions of the temperature T. Consequently, for any function F, we have

$$F = a_0 + a_1 T. \tag{16}$$

Values of a_0 and a_1 for solid and liquid Al(7075) are shown in Table 2. All values are in the appropriate international system (SI) units.

Melting was assumed to occur between values of temperature given by $T_i = 750\ K$ and $T_f = 908\ K$. At temperatures below T_i, solid properties were used, while at temperatures above T_f, liquid properties were used. At intermediate values of T, i.e., for the solid-liquid mixture, the property in question was scaled linearly with T between the value for the solid at T_i and for the liquid at T_f.

Table 2. Values of Coefficients for Material Properties of Al(7075)

	Solid		Liquid	
Property	a_0	a_1	a_0	a_1
C	645.0	0.705	1302.0	0
η_r	1.42×10^{-8}	1.36×10^{-10}	1.51×10^{-7}	1.33×10^{-10}
κ	247.0	-6.92×10^{-2}	93.0	0
ρ	2851.0	-0.5	2294.0	0

During the time that melting is occurring at some location in the armature, an amount of energy per unit volume and time E_L is required to convert solid to liquid. Generally, this energy is represented by the relation

$$E_L = \rho L F(T) \frac{\partial T}{\partial t}, \tag{17}$$

where L denotes the latent heat of fusion and F is a function that corresponds to the amount of liquid produced per unit rise in temperature of the solid-liquid mixture. For most metallic elements, melting takes place at a well-defined temperature so that F can be represented as a delta function, $\delta(T - T_m)$, in which T_m is the melting temperature. For most armature materials, however, melting occurs over a range in temperature, i.e., between T_i and T_f, and the function F is not known with any accuracy. We make the same assumption as in our previous work that this function can be represented as

$$F(T) = \frac{1}{\pi} \frac{\varepsilon}{(T - T_{av})^2 + \varepsilon^2}, \tag{18}$$

where $T_{av} = (T_i + T_f)/2$ and ε is chosen so that the function suitably peaks about T_{av}. This particular choice is not unique, but it seems reasonable until more definitive information is known; furthermore, it approaches the delta function in the limit that ε approaches zero. In our actual calculations, we chose $\varepsilon = (T_f - T_i)/6$; we have demonstrated previously that this choice implies that about 90% of the latent heat is absorbed in the relevant temperature range. The latent heat is taken as $L = 4 \times 10^5 \ J/kg$.

2.4 Numerical Solution

The numerical solution of Equations (12) and (13) is performed in the following manner. A non-uniform rectangular grid in the computational space of ξ and η is generated. The grid points are clustered so as to achieve a relatively fine grid in the physical space of x an y in regions where significant spatial variations occur. Such a region might correspond, for example, to the left-hand edge of the armature where diffusion is initiated and where substantial curvature in the surface occurs. The equations are then solved in the computational space, and the results are again transformed into the physical space for analysis and presentation.

The numerical technique that is applied to solve Equations (12) and (13) has been described in earlier work (Powell, Walbert, & Zielinski 1993) and is not described in detail here. In brief, all derivatives are represented by standard finite differences, and the resulting nonlinear equations are solved by iteration (Ames 1997). Some specific grids employed are discussed subsequently. Typically, a time step of 50 to 100 *ns* proves satisfactory.

3. Calculations

We now describe results of seven calculations in which we have varied the input parameters α, β, and r_0 and have endeavored to determine the effect of that variation on heating in the vicinity of the root radius [i.e., (x_1,y_1) to (x_2,y_2)]. In all calculations, the other input parameters were kept constant at the following values: $L = 10\,cm$, $h = 38\,mm$, and $y_0 = 18\,mm$. Values of α, β, and r_0 are summarized for the various cases in Table 3. In Cases 2 and 3, r_0 was varied relative to the value in the baseline case, Case 1, while α and β were held constant; in Cases 4 and 5, the angle α was varied while r_0 and β were held constant; and in Cases 6 and 7, the angle β was varied while r_0 and α were held constant. Also indicated in the table are values for the other parameters in Table 1 (i.e., x_1, x_2, y_1, y_2, x_3,and x_0) that change as a result of the variation in α, β, and r_0.

Table 3. Input Parameters for Various Calculations

Input Parameter	Case 1	Case 2	Case 3	Case 4	Case 5	Case 6	Case 7
$r_0\,(mm)$	3.5	2.0	5.0	3.5	3.5	3.5	3.5
$\alpha\,(deg.)$	18	18	18	12	24	18	18
$\beta\,(deg.)$	12	12	12	12	12	8	16
$x_1\,(mm)$	51.31	55.70	46.92	77.98	37.74	51.31	51.31
$x_2\,(mm)$	50.96	55.50	46.41	77.98	37.04	50.71	51.19
$y_1\,(mm)$	21.33	19.90	22.76	21.42	21.20	21.33	21.33
$y_2\,(mm)$	14.58	16.04	13.11	14.58	14.58	14.53	14.64
$x_0\,(mm)$	50.23	55.08	45.37	77.26	36.32	50.23	50.23
$x_3\,(mm)$	-17.62	-19.98	-15.26	9.41	-31.53	-52.70	0.15

The current per unit height along the z direction (i.e., the height of the rail) was also the same for each calculation and was taken to be of the form

$$j = j_0 \sin(\pi t / t_0). \tag{19}$$

In this equation, t_0 is the acceleration time and the time when the current goes to zero. The amplitude j_0 was chosen so that this 2-D model would have produced a final velocity of the armature of v_f for a given h and m', where m' is the armature mass per unit length along the z direction. For the assumed values of $h = 38\,mm$, $m' = 20\,kg/m$, and $v_f = 2.3\,km/s$, we found that $j_0 \cong 2.7\times10^7\,A/m$.

Reasonable corroboration between modeling and experimental results has previously been obtained via this scaling procedure (Powell & Zielinski 1995). For a real 3-D railgun, in which the in-bore fields are smaller on average than for the 2-D case, a higher value of j_0 (by about a factor of 2) would be required to achieve the same acceleration.

Shown in Figure 3 is a typical physical space grid employed in the calculation for Case 1. As was pointed out previously, this grid was generated from a rectangular computational space grid that had a non-uniform grid spacing. In particular, the grid was chosen so that $\Delta\xi$ was small near the left-hand edge of the armature where diffusion initiates, and $\Delta\eta$ was small in the vicinity of the root radius. The grid shown in Figure 3 contains 80 points in the x direction and 70 in the y direction. We have, however, used both larger and smaller grids to perform the calculations. The largest grids employed contained about 2,500 grid points and gave satisfactory results except at very small, localized regions where there was a transition from a straight line segment to a curved segment. These discrepancies could probably have been eliminated with fewer points clustered more judiciously.

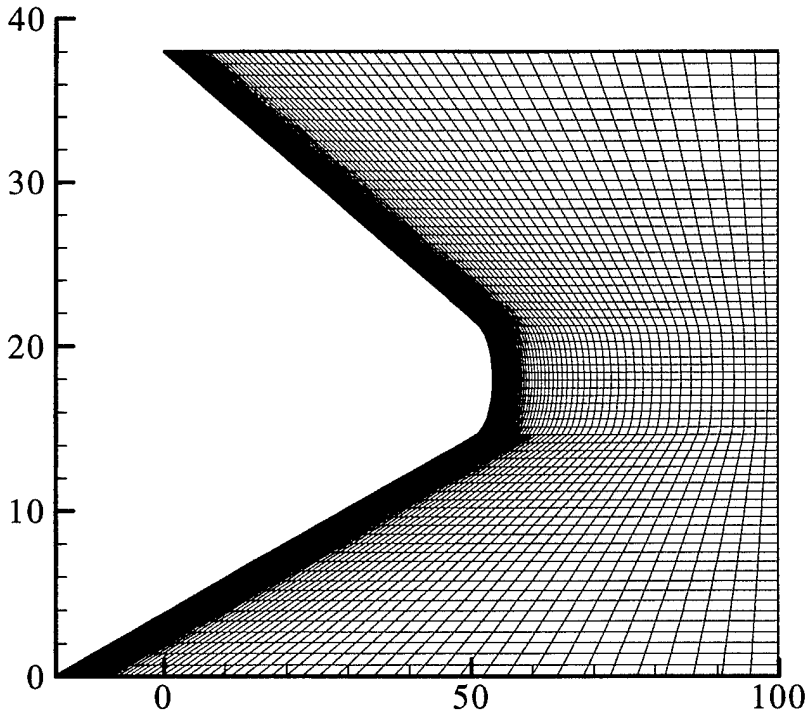

Figure 3. Physical Space Grid for Case 1.

In Figure 4 are plotted lines of constant magnetic induction at the time of maximum current, namely, 1.3 *ms*. It is possible to prove from Maxwell's

equations that current cannot cross these lines, so they can also be taken to represent current streamlines. Eleven such streamlines are shown in the figure (counting the left- and right-hand boundaries), so 10% of the total current is contained between successive lines. It is evident that the current has not yet diffused through the armature at this early time and is still confined largely to the left-hand side. The current density is high in the vicinity of the root radius, as can be seen from the proximity of the streamlines. This high current density results from current being conducted around a "corner" for which the angle measured in the conductor is greater than 180 degrees. It is also evident that the current density is relatively small along the left-hand edge near the centerline ($y = 0$) and near the top ($y = h$). The small current density in these regions results from conduction past corners in which the angle is smaller than 180 degrees. We have discussed how conduction occurs at these large- and small-angle corners in much of our previous work and we discuss it in some greater detail when we present results of the other calculations.

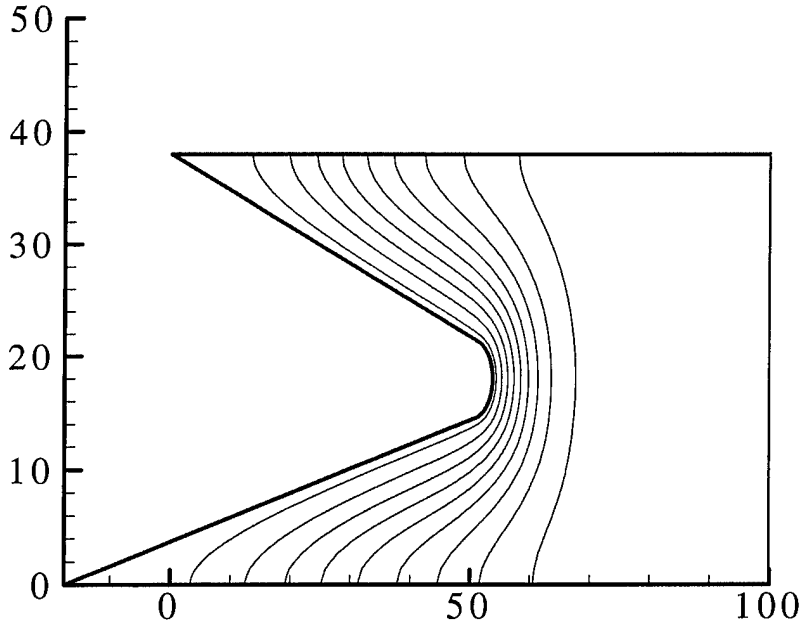

Figure 4. Current Steamlines in Armature at t = 1.3 *ms* for Case 1.

Isotherms at the end of the calculation (i.e., at 2.6 *ms*) are shown in Figure 5. The isotherms demonstrate the effect of the high and low current density discussed in relation to Figure 4. In particular, there is evidence of substantial heating in the vicinity of the root radius. A small area around that location has reached the incipient melting temperature of 750 K. Similarly, the corners at the top and along the centerline are relatively cool.

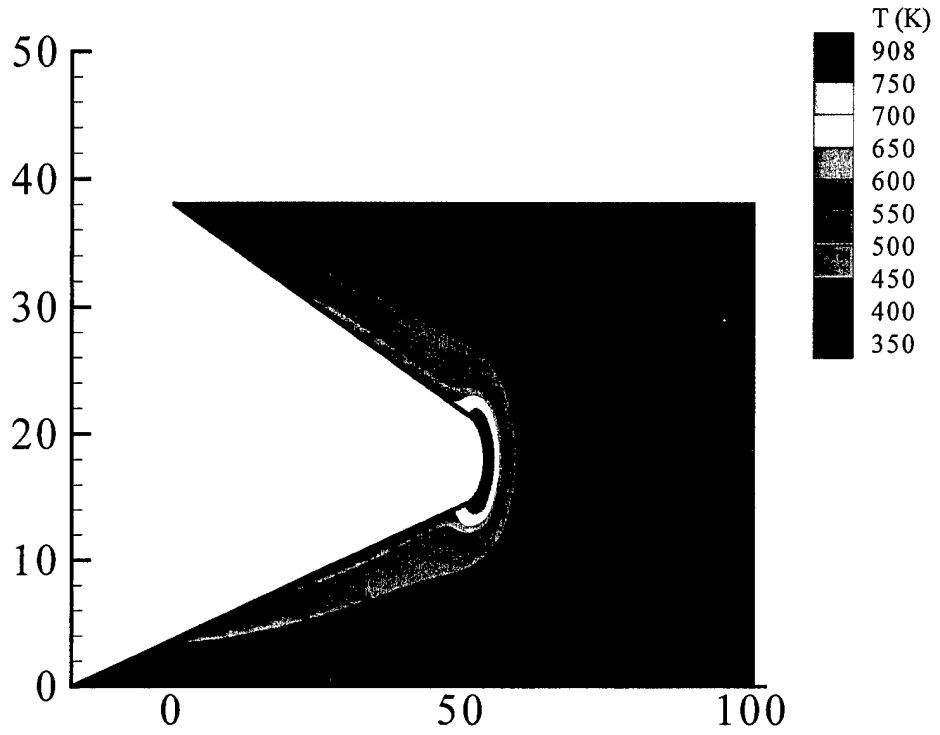

Figure 5. Isotherms in Armature at 2.6 *ms* for Case 1.

Results for the remaining six calculations are qualitatively similar and are not discussed in detail. Consequently, we plot for each of the calculations only the temperature along the left-hand edge of the armature, T_s, as a function of the coordinate y, and the temperature as a function of the horizontal distance Δx from the edge of the armature into the armature along the line $y = y_0$. The plots are presented in groups containing three cases: Cases 1, 2, and 3 (r_0 varies); Cases 1, 4, and 5 (α varies); and Cases 1, 6, and 7 (β varies).

In Figures 6 and 7 are presented the plots just described for Cases 1, 2, and 3. As expected, the heating in the vicinity of the root radius increases with decreasing values of r_0. This behavior arises because as current is conducted around a convex surface such as the root radius, diffusion arising at one localized point on the surface does not overlap with that arising at another. Consequently, diffusion away from the surface is difficult, the streamlines remain closely confined, and the current density is high. This situation may be compared with one in which current is conducted along a concave surface. Then the skin effects from localized points do overlap, and the fields and current diffuse easily. This description is analogous to conduction around corners in which the angle in the conductor is greater than 180 degrees (convex surface) or less than 180 degrees (concave surface), as explained in our earlier work. It is noteworthy from Figure 7 that the temperature drops to near ambient at a distance of about 15 *mm* from the edge of

the armature in each of the three cases. In addition, the temperature is nearly the same for each case at distances of about 5 *mm* or greater. Clearly, at these distances, the details of the root radius cannot be "seen"; rather, the current appears to have come from two lines L_1 and L_2 that intersect at an angle given by $\alpha+\beta$. The significant variations in slope of the curve for Case 2 near the surface ($\Delta x = 0$) appear to result from absorption of the heat of fusion that occurs predominantly in the temperature range between 750 *K* and 908 *K*, followed by the more rapid heating that occurs after 908 *K*. The more rapid heating occurs because the resistivity of the liquid is higher than that of the solid. In Cases 1 and 3, the temperature does not exceed 908 *K*.

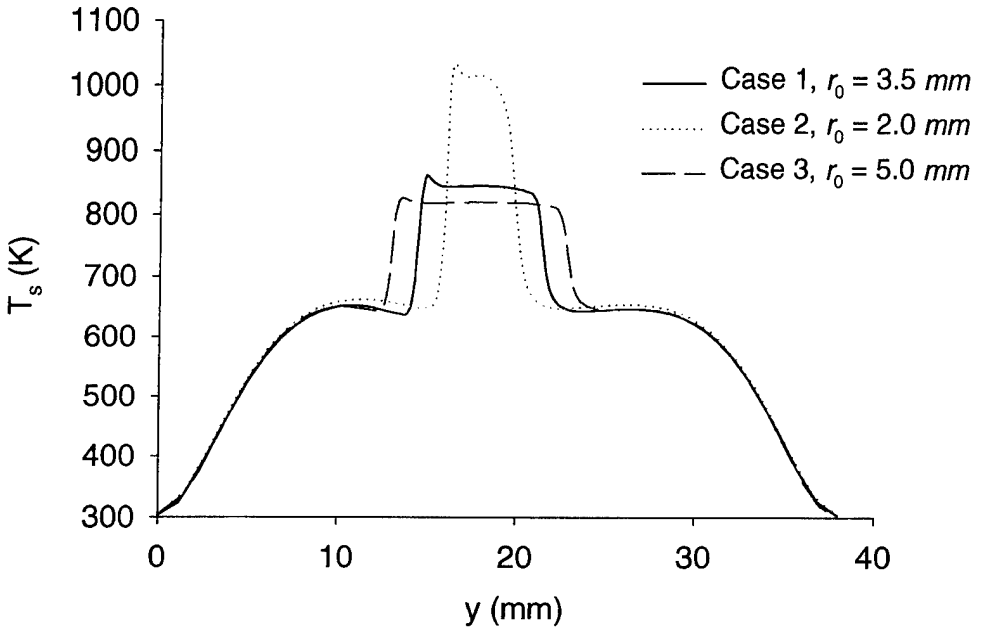

Figure 6. Final Temperature Along the Left-Hand Surface of Armature Versus y for Cases 1, 2, and 3.

In Figures 8 and 9 are shown results for Cases 4 and 5, which correspond to those just discussed. In Cases 4 and 5, the angle α was varied from its value in Case 1, while r_0 and β were held constant. Clearly, there is virtually no dependence on α for these cases. Presumably, the radius r_0 is sufficiently large and the points (x_1,y_1) and (x_2,y_2) (where the straight line segments begin) are sufficiently far removed from the line at $y = y_0$ that the changes in the surface structure at those points do not affect the results. Such a conclusion might not hold for values of r_0 sufficiently small that the origins of the straight line segments were not so far removed. Identical conclusions can be drawn for Cases 6 and 7 in which the angle β was varied. Those results are evident in Figures 10 and 11.

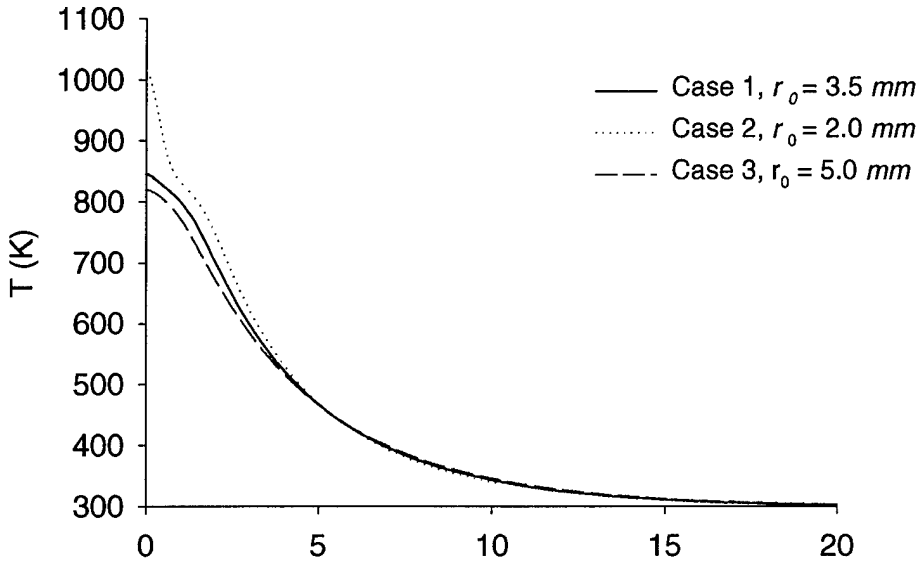

Figure 7. Final Temperature Versus Distance From Armature Surface Along the Horizontal Line $y = y_0$ for Cases 1, 2, and 3.

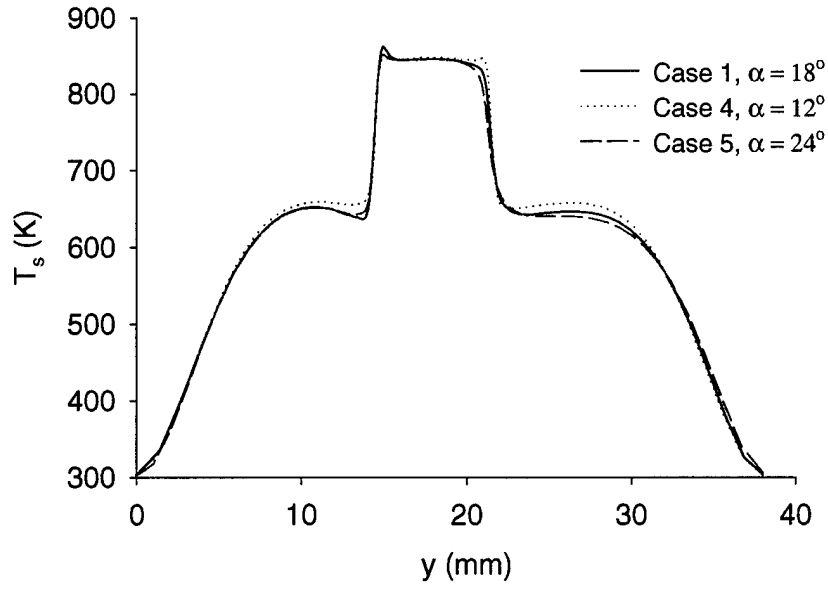

Figure 8. Final Temperature Along the Left-Hand Surface of Armature Versus y for Cases 1, 4, and 5.

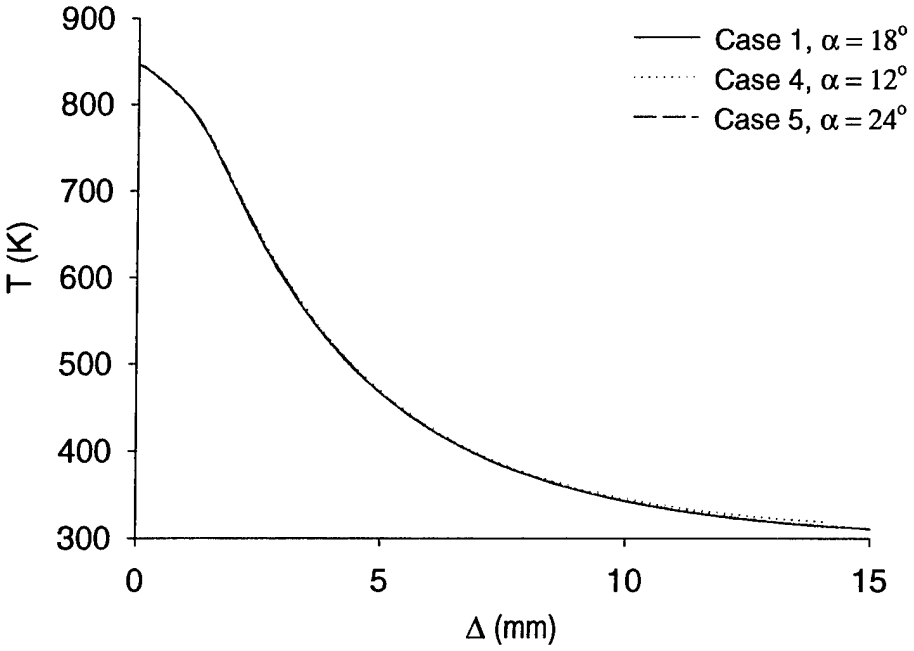

Figure 9. Final Temperature Versus Distance From Armature Surface Along the Horizontal Line $y = y_0$ for Cases 1, 4, and 5.

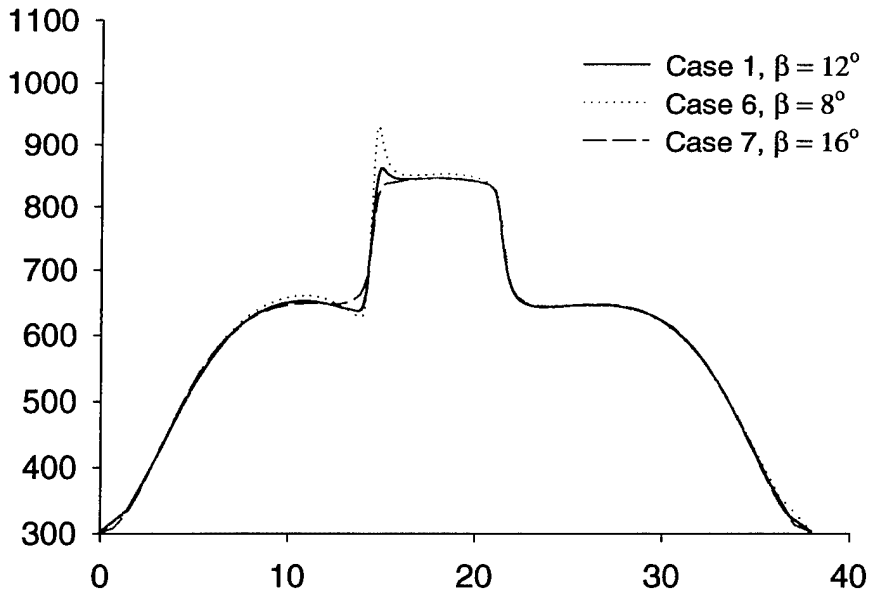

Figure 10. Final Temperature Along the Left-Hand Surface of Armature Versus y for Cases 1, 6, and 7.

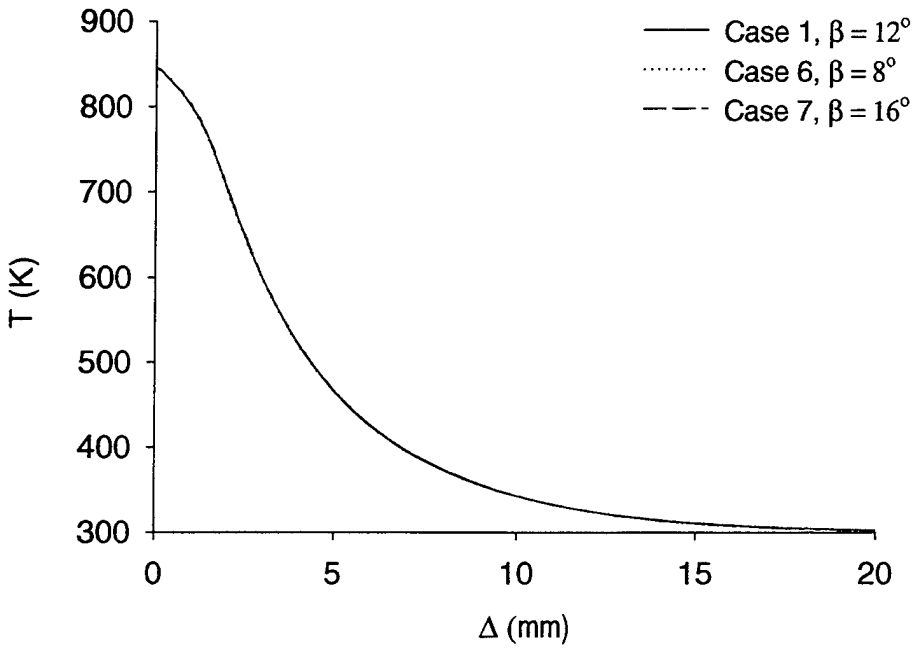

Figure 11. Final Temperature Versus Distance From Armature Surface Along the Horizontal Line $y = y_0$ for Cases 1, 6, and 7.

4. Summary and Conclusions

A simplified version of a time- and position-dependent solution for current and heat transport in a solid armature has been solved. Unlike in previous work, the motion of the armature and its resultant influence on current flow at the rail-armature interface were neglected. This simplification dramatically reduces the solution time of the problem and is not expected to affect the results in the region of interest, namely, at points removed from the rail-armature interface.

Solutions predicting the temperature in the armature at the time of exit indicate that the angle of the rear surfaces (within the rather large allowable design space of 8 to 24 degrees) does not appreciably affect the heating at the root radius. That such a dependence might exist was a previously identified source of concern. However, as expected, the generation of the thermal load is rather sensitive to the radius of the root region. The load increases dramatically for radii of less than about 2 *mm*.

Future work will employ the full 2-D solution for a moving armature and rail conductor system. In addition, a current pulse that is representative of a more realistic pulsed power supply will be used.

INTENTIONALLY LEFT BLANK

5. References

Ames, W.F., "Numerical Methods for Partial Differential Equations," New York: Academic, Chapter 5, 1997.

Hsieh, K.T., "A Lagrangian Formulation for Mechanically, Thermally Coupled Electromagnetic Diffusive Processes with Moving Conductors," *IEEE Transactions on Magnetics*, Vol. 31, p. 604, 1995.

Long, G.C., "Railgun Current Density Distributions," *IEEE Transactions on Magnetics*, Vol. 22, p. 1597, 1986.

Long, G.C., "Fundamental Limits to the Velocity of Solid Armatures in Railguns," Doctoral Dissertation, University of Texas at Austin, Publication Number TD-35, 1987.

Newill, J.F., A.E. Zielinski, and J.D. Powell, "Coupled Structural and Electromagnetic Computations for Hypervelocity Projecile Dynamics." ARL-TR, to be published.

Powell, J.D., D.J. Walbert, and A.E. Zielinski, "Two-Dimensional Model for Current and Heat Transport in Solid-Armature Railguns," ARL-TR-74, U.S. Army Research Laboratory, Aberdeen Proving Ground, MD, February 1993.

Powell, J.D., and A.E. Zielinski, "Current and Heat Transport in the Solid-Armature Railgun," *IEEE Transactions on Magnetics*, Vol. 31, p. 645, 1995.

Powell, J.D., and A.E. Zielinski, "Current and Heat Transport in the Cannon-Caliber Electromagnetic Gun Armature," ARL-MR-258, U.S. Army Research Laboratory, Aberdeen Proving Ground, MD, 1995.

Powell, J.D., and A.E. Zielinski, "A Preliminary Study of Wear in the Solid-Armature Railgun," IAT.R 0155, Institute for Advanced Technology, The University of Texas at Austin, 1997.

Powell, J.D., and A.E. Zielinski, "Observation and Simulation of Solid-Armature Railgun Performance," *IEEE Transactions on Magnetics*, Vol. 35, p. 84, 1999.

Rodger, D., P.J. Leonard, and J.F. Eastman, "Modeling Electromagnetic Rail Launchers at Speed Using 3D Finite Elements," IEEE Transactions on Magnetics, Vol. 27, p. 314, 1991.

Zielinski, A., "Integrated Launch Package Design with Considerations for Reduced Scale Demonstration," ARL-TR, U.S. Army Research Laboratory, Aberdeen Proving Ground, MD, to be published.

NO. OF COPIES	ORGANIZATION
1	ADMINISTRATOR DEFENSE TECHNICAL INFO CTR ATTN DTIC OCA 8725 JOHN J KINGMAN RD STE 0944 FT BELVOIR VA 22060-6218
1	DIRECTOR US ARMY RSCH LABORATORY ATTN AMSRL CI AI R REC MGMT 2800 POWDER MILL RD ADELPHI MD 20783-1197
1	DIRECTOR US ARMY RSCH LABORATORY ATTN AMSRL CI LL TECH LIB 2800 POWDER MILL RD ADELPHI MD 20783-1197
1	DIRECTOR US ARMY RSCH LABORATORY ATTN AMSRL D D SMITH 2800 POWDER MILL RD ADELPHI MD 20783-1197
1	DIR FOR THE DIRECTORATE OF FORCE DEVELOPMENT US ARMY ARMOR CTR ATTN COL E BRYLA FT KNOX KY 40121-5000
1	US ARMY MATERIEL CMD ATTN AMC DCG T 5001 EISENHOWER AVE ALEXANDRIA VA 22333-0001
1	US ARMY MISSILE CMD ATTN AMSMI RD W MCCORKLE REDSTONE ARSENAL AL 35898-5240
2	US ARMY TACOM TARDEC ATTN AMSTA TR D MS #207 J CHAPIN M TOURNER WARREN MI 48397-5000
1	US ARMY TACOM-ARDEC ATTN FSAE GCSS TMA J BENNETT BLDG 354 PICATINNY ARSENAL NJ 07806-5000

NO. OF COPIES	ORGANIZATION
6	INST FOR ADVANCED TECH UNIV OF TEXAS AT AUSTIN ATTN P SULLIVAN F STEPHANI T WATT W REINCKE D BARNETT M ERENGIL 3925 W BRAKER LANE STE 400 AUSTIN TX 78759-5316
3	UNIV OF TEXAS AT AUSTIN CTR FOR ELECT PRC MAIL CODE R7000 ATTN A WALLS J PAPPAS J KITZMILLER S PRATAP AUSTIN TX 78712
2	LOCKHEED-MARTIN-VOUGHT ATTN N WELLS K COOK MS WT-21 PO BOX 650003 DALLAS TX 75265-0003
1	INST FOR DEF ANALYSIS ATTN I KOHLBERG 1801 N BEAUREGARD ST ALEXANDRIA VA 22311
1	KAMAN ELECTROMAGNETICS CORP ATTN P MONGEAU 2 FOX RD HUDSON MA 01749
2	UNIV AT BUFFALO SUNY/AB ATTN J SARJEANT PO BOX 601900 BUFFALO NY 14260-1900
3	UDLP ATTN MS M170 B GOODELL R JOHNSON 4800 E RIVER RD MINNEAPOLIS MN 55421-1498
1	UNIV OF TEXAS AT AUSTIN ATTN M DRIGA ENS 434 DEPT OF ECE MAIL CODE 60803 AUSTIN TX 78712

NO. OF COPIES ORGANIZATION

1 SAIC
ATTN G CHRYSSOMALLIS
3800 W 80TH ST STE 1090
BLOOMINGTON MN 55431

2 SAIC
ATTN J BATTEH L THORNHILL
4901 OLDE TOWNE PKWY STE 200
MARIETTA GA 30068

1 SAIC
ATTN K A JAMISON
1247 B N EGLIN PKWY
SHALIMAR FL 32579

2 IAP RSCH INC
ATTN D BAUER J BARBER
2763 CULVER AVE
DAYTON OH 45429-3723

3 MAXWELL TECHNOLOGIES
ATTN P REIDY T WOLFE
9244 BALBOA AVE
SAN DIEGO CA 92123

1 NC STATE UNIV
DEPT OF NUCLEAR ENGR
ATTN M BOURHAM
BOX 7909
RALEIGH NC 27695-7909

1 MAXWELL PHYSICS INTERNATL
ATTN C GILMAN
2700 MERCED ST
PO BOX 5010
SAN LEANDRO CA 94577-0599

1 ATA ASSOCIATES
ATTN W ISBELL
PO BOX 6570
SANTA BARBARA CA 93160-6570

ABERDEEN PROVING GROUND

2 DIRECTOR
US ARMY RSCH LABORATORY
ATTN AMSRL CI LP (TECH LIB)
BLDG 305 APG AA

NO. OF COPIES ORGANIZATION

4 DIRECTOR
US ARMY RSCH LABORATORY
ATTN AMSRL WM J SMITH
AMSRL WM B A HORST
B FORCH D LYON
BLDG 4600

20 DIRECTOR
US ARMY RSCH LABORATORY
ATTN AMSRL WM BC
P PLOSTINS J GARNER
V OSKAY M BUNDY
G COOPER J SAHU
P WEINACHT H EDGE
B GUIDOS D WEBB
A ZIELINSKI (5 CYS)
K SOENCKSEN
S WILKERSON
T ERLINE J NEWILL
M DELGUERCIO
BLDG

1 DIRECTOR
US ARMY RSCH LABORATORY
ATTN AMSRL WM T B BURNS
BLDG

1 DIRECTOR
US ARMY RSCH LABORATORY
ATTN AMSRL WM TA M KEELE
BLDG

10 DIRECTOR
US ARMY RSCH LABORATORY
ATTN AMSRL WM TE A NIILER
P BERNING C HUMMER
T KOTTKE J POWELL (5 CYS)
G THOMSON
BLDG 120

REPORT DOCUMENTATION PAGE

Form Approved
OMB No. 0704-0188

1. AGENCY USE ONLY *(Leave blank)*	2. REPORT DATE	3. REPORT TYPE AND DATES COVERED
	July 2001	Final

4. TITLE AND SUBTITLE
Current and Heat Transport in a Double Taper Sabot-Armature

5. FUNDING NUMBERS
PR: 1L162618AH80

6. AUTHOR(S)
Powell, J.D.; Zielinski, A.E. (both of ARL)

7. PERFORMING ORGANIZATION NAME(S) AND ADDRESS(ES)
U.S. Army Research Laboratory
Weapons & Materials Research Directorate
Aberdeen Proving Ground, MD 21005-5066

8. PERFORMING ORGANIZATION REPORT NUMBER

9. SPONSORING/MONITORING AGENCY NAME(S) AND ADDRESS(ES)
U.S. Army Research Laboratory
Weapons & Materials Research Directorate
Aberdeen Proving Ground, MD 21005-5066

10. SPONSORING/MONITORING AGENCY REPORT NUMBER
ARL-TR-2523

11. SUPPLEMENTARY NOTES

12a. DISTRIBUTION/AVAILABILITY STATEMENT
Approved for public release; distribution is unlimited.

12b. DISTRIBUTION CODE

13. ABSTRACT *(Maximum 200 words)*

A model developed previously to investigate the transport of electromagnetic fields and energy in solid-armature railguns is simplified to exclusively study heating within the interior of the armature. A particular type of armature is then specifically studied, and the effect of variation of a number of parameters that affect its geometry is investigated. Results of the calculations are studied carefully and explained by basic physical principles. Some indication of how the results and conclusions can be used to influence design criteria for armatures is also indicated.

14. SUBJECT TERMS
electromagnetic gun
electromagnetic launch
electromagnetic propulsion
rail gun

15. NUMBER OF PAGES
30

16. PRICE CODE

17. SECURITY CLASSIFICATION OF REPORT	18. SECURITY CLASSIFICATION OF THIS PAGE	19. SECURITY CLASSIFICATION OF ABSTRACT	20. LIMITATION OF ABSTRACT
Unclassified	Unclassified	Unclassified	